A possible auroral signature of a magnetotail reconnection process on Jupiter

D. Grodent,[1] J.-C. Gérard,[1] J. T. Clarke,[2] G. R. Gladstone,[3] and J. H. Waite Jr.[4]

Received 3 December 2003; revised 3 February 2004; accepted 8 March 2004; published 1 May 2004.

[1] Several theoretical models and in situ observations consistently suggest that the process of nightside reconnection associated with Earth's magnetospheric substorms is also taking place in the midnight tail region of Jupiter. We report the observation of a new auroral feature which takes the form of isolated spots appearing near the northern dusk-midnight limb, poleward of the main auroral oval. This feature was clearly detected in three HST-STIS data sets obtained on 14, 16, and 18 December 2000. Its position poleward of the main auroral oval, and lagging corotation, shows that it is magnetically connected to a distant region of the nightside magnetosphere. It is therefore suggested that these transient spots are the auroral signatures of reconnection processes occurring in the nightside tail of the distant Jovian magnetosphere. The cause of this reconnection is somewhat analogous to the case of a solar coronal mass ejection, so one may refer to it as a "Jovian mass ejection." *INDEX TERMS:* 6220 Planetology: Solar System Objects: Jupiter; 2704 Magnetospheric Physics: Auroral phenomena (2407); 2756 Magnetospheric Physics: Planetary magnetospheres (5443, 5737, 6030); 2788 Magnetospheric Physics: Storms and substorms; *KEYWORDS:* aurora, Jupiter, reconnection

Citation: Grodent, D., J.-C. Gérard, J. T. Clarke, G. R. Gladstone, and J. H. Waite Jr. (2004), A possible auroral signature of a magnetotail reconnection process on Jupiter, *J. Geophys. Res.*, *109*, A05201, doi:10.1029/2003JA010341.

1. Introduction

[2] The Pioneer, Voyager, and Ulysses missions have shown that the general picture of the Jovian nightside magnetosphere is in several respects similar to the Earth's magnetotail. It consists of a plasma sheet with an embedded current sheet stretching out far into the antisunward direction. *Vasyliũnas* [1983] and *Nishida* [1983] suggested that tail reconnection processes similar to the terrestrial case may also exist in the Jovian magnetosphere. In the picture proposed by *Carbary et al.* [1976] and *Vasyliũnas* [1983], magnetic flux tubes are loaded with heavy ions originating from the moon Io. They are pulled outward by centrifugal force and pressure anisotropies [*Paranicas et al.*, 1991] as the newly created ions are brought to corotation. At some distance on the nightside, the stretching of the flux tubes is such that oppositely directed magnetic field lines reconnect across a thin portion of the current sheet. During this reconnection process a plasmoid may be released down the tail, allowing plasma, continuously produced deep inside the magnetosphere near Io's orbit, to escape from the Jovian magnetosphere.

[3] The Galileo spacecraft found localized regions of strong northward and southward field components beyond about 50 R_J in the postmidnight, predawn sector of the Jovian magnetosphere. *Russell et al.* [1998] interpreted them as localized transient reconnections in a rapidly rotating magnetized plasma. *Russell et al.* [1998] discuss two events characterized by an abrupt rise of the normal component of the magnetic field which lasted about an hour. They estimated the size of the disturbed region to be $\sim$25 $R_J \times$ 25 R_J. These disturbances thus appear to be large but not global events and may represent only a fraction of the reconnection taking place in the magnetodisk. Following further analysis of the Galileo observations, *Russell et al.* [2000] noted that small events occur irregularly but on average about every 4 hours and large events about once a day in a region beyond 50 R_J and from midnight to 0300LT. During orbit G12 in 1996, the Galileo spacecraft detected a number of particle bursts with large radial/antisunward anisotropies in the distant Jovian magnetotail. *Woch et al.* [1999] analyzed one such jet of energetic particles propagating in the radial direction and reported signatures which, at Earth, are commonly interpreted as the formation of active X-lines and an associated release of a plasmoid. Statistical analysis of the burst events appearing in the Galileo observations [*Woch et al.*, 2002] shows that they are concentrated in the postmidnight deep tail region. The transition from mainly inward to mainly outward directed bursts occurs at roughly 70 R_J in the predawn region and at 120 R_J

[1]Laboratory for Planetary and Atmospheric Physics, Université de Liège, Liège, Belgium.
[2]Center for Space Physics, Boston University, Boston, Massachusetts, USA.
[3]Southwest Research Institute, San Antonio, Texas, USA.
[4]Space Physics Research Laboratory, University of Michigan, Ann Arbor, Michigan, USA.

0148-0227/04/2003JA010341$09.00

around local midnight. The transition establishes the most probable location of a neutral line. The continuation of this line to the premidnight/dusk sector is unknown, due to a poor coverage of this sector by Galileo. The process appears to be of a transient, impulsive nature rather than a continuous, steady state process. The burst events show a tendency to recur every 2 to 3 days. The ion and electron energy spectra during the bursts show evidence for heating or acceleration of particles. Lasting several tens of minutes to a few hours and thus being relatively short in duration, these burst events are part of a large scale instability of the Jovian magnetotail which takes several planetary rotations to develop. *Woch et al.* [2002] suggest that the particle flow burst events are part of the source process of the auroral dawn storms and auroral flares observed with the HST. However, the energy density carried by the inward beams of accelerated particles is too low to account for auroral emissions of the reported extreme intensity of the dawn storms. Therefore *Woch et al.* [2002] suggest that breakup of the magnetic topology of the tail associated with the bursts leads to a disruption of the cross tail current. In analogy to auroral substorms at Earth, the current will be partly diverted into the ionosphere and will drive intense auroral events. *Louarn et al.* [1998, 2000] have reported the quasiperiodic occurrence of "energetic magnetospheric events" corresponding to enhancements of the various Jovian radio emissions observed by Galileo. These sporadic phenomena are closely associated with the dynamic events described by *Woch et al.* [1999] and are recurring with a frequency varying from 2.5 days to more than 4 days, with quiet periods of 10 days. They have been associated with sudden and periodic plasma loading of the depleted Jovian magnetodisk due to instabilities occurring in the outer part of the Io torus. This feeding phase is followed by a progressive outward plasma transport which likely looses iogenic material to the tail.

[4] Earlier ultraviolet (UV) images of Jupiter's aurora have shown highly variable emissions inside the polar regions [*Prangé et al.*, 1995; *Clarke et al.*, 1998; *Waite et al.*, 2001; *Grodent et al.*, 2003b], but none so far has reported on discrete emissions from the midnight sector poleward of the main oval. In this study, we describe a new auroral feature forming isolated spots appearing near the northern dusk-midnight limb, poleward of the main auroral oval. We suggest that this feature represents the auroral signature of reconnection processes occurring in the nightside tail of the Jovian magnetosphere.

2. Observations

[5] During the winter of 2000–2001, the photon-counting detector MAMA (Multi-Anode Micro channel Array) of the STIS camera (Space Telescope Imaging Spectrograph) on board the Hubble Space Telescope obtained approximately 200 far-ultraviolet images of the auroral emission near Jupiter's poles. These observations were completed directly before and after Cassini's closest approach of Jupiter on 30 December 2000. They span a period of six weeks extending from 14 December 2000 to 21 January 2001 (see *Grodent et al.* [2003a] for a full description of the data set and of its reduction). The MAMA array consists of 1024×1024 pixels providing a field of view of $24.7'' \times 24.7''$ with a $\sim 0.08''$ full width at half maximum point spread function (PSF). For a direct comparison, the images were all scaled in pixel size to display Jupiter as it would appear at a distance of 4.2 Astronomical Units. The transverse distance subtended by one $0.02''$ pixel at Jupiter is then $\sim$74 km. The images were accumulated for $\sim$100 s, during which Jupiter rotates by $\sim 1^\circ$. This rotation introduces a small smearing of the images which, for a surface feature located near the limb at a high latitude ($\geq 70^\circ$) is less than the size of a pixel and has therefore been ignored.

[6] The viewing geometry for the southern aurora is less favorable for Earth-based observations of Jupiter's aurora. The proximity of the magnetic south pole to the spin axis and the northern subsolar latitude restricted the view of the auroral distribution compared to the north aurora. As a result, the dusk-nightside portion of the main oval is not visible on the images of the southern aurora and we put the emphasis on the images taken in the north. However, it should be at least mentioned that, although there is no definite evidence for polar spots in the south, localized brightenings are observed at the limb which could result from the limb brightening of emission features, a few degrees poleward of the main oval, so that north-south conjugacy may not be directly ruled out.

2.1. Overall Auroral Morphology

[7] The morphology of the Jovian UV auroral emission is usually described in terms of three major components: the satellite footprints, the main oval, and the polar emissions [e.g., *Grodent et al.*, 2003a, 2003b]. These three components are well apparent in Figure 1 which shows the same northern auroral region on the three days during which the new feature was clearly visible at the dusk-midnight limb.

[8] The satellite auroral footprints are easily identified by the fact that they remain fixed along magnetic flux tubes connected to Io, Europa, and Ganymede [*Clarke et al.*, 2002]. The Io footprint is the most conspicuous one, it appears as a small and bright spot ($\sim$200 kiloRayleighs of H_2 Lyman and Werner band emission [kR]) followed by a long tail, trailing downstream along the footprint of the field lines passing through the orbit of Io.

[9] The main auroral oval forms a relatively stable strip of emission which closes around the magnetic pole. In the northern hemisphere, at longitudes greater than 180° (all longitudes cited in this paper are System III longitudes), the emission is almost always very narrow ($\sim$1000 km), while at smaller longitudes the emission broadens and tends to break from the main oval. It should be noted that this overall morphology is compatible with the auroral structures observed in the infrared [e.g., *Satoh et al.*, 1996; *Stallard et al.*, 2003], although they do not stem from the same processes, and *Vasavada et al.* [1999] also reported local time variations of the morphology and total width of the main oval observed in visible wavelengths from the Galileo spacecraft. The brightness observed in the main oval varies from $\sim$50 to $\sim$500 kR. It is generally accepted that the main auroral oval is connected with the magnetosphere-ionosphere coupling current system associated with the breakdown of rigid corotation in the middle

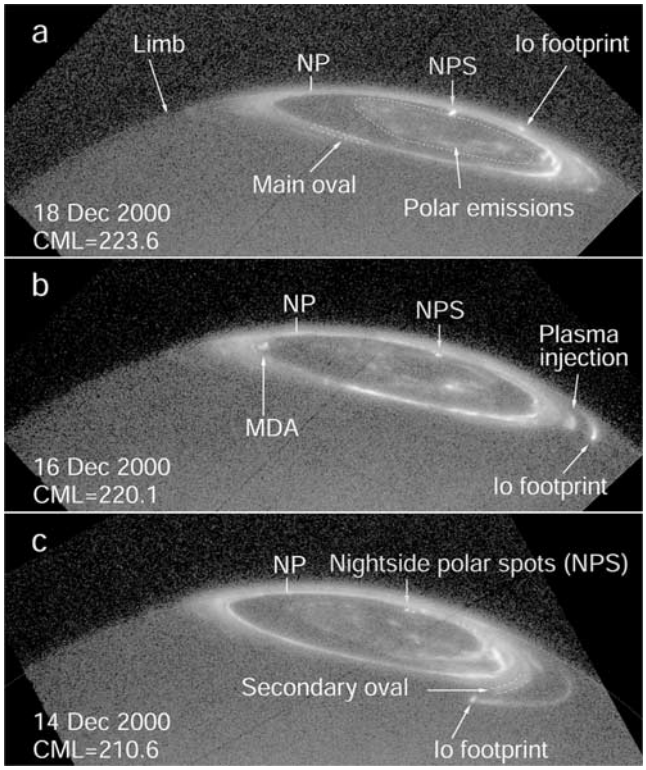

Figure 1. HST-STIS images of the northern polar region of Jupiter showing the new auroral feature, which we refer to as nightside polar spots (NPS) (indicated by an arrow). The three far-UV images were taken on (a) 18 December 2000, (b) 16 December 2000, and (c) 14 December 2000. They were accumulated for ~100 s with the FUV-MAMA Clear aperture. The CML is about 220° for each image, so that the auroral morphologies are very similar, apart from the Io footprint, which has a period of 42 hours. The main oval, the secondary oval, and the polar emissions are located with dashed lines and/or arrows. The plasma injection signature and the multiple dawn arcs (MDA) are visible in Figure 1b only. The north pole (NP) is marked with a vertical tick, and the planetary limb is highlighted with a thin dotted line. See color version of this figure at back of this issue.

magnetosphere region. The main auroral oval may result from the upward Birkeland current that enforces partial corotation of the outward moving iogenic plasma [e.g., *Bunce and Cowley*, 2001; *Hill*, 2001]. According to this interpretation, the equatorial source of these outward field-aligned currents is broadly distributed within the middle magnetosphere current sheet, between inner distances of ~20 R_J and outer distances of several tens of R_J, bounded by the radial extent of the current sheet.

[10] The polar emissions, i.e., the emission appearing poleward of the main oval (highlighted with a dotted contour in Figure 1a), by contrast, vary rapidly [*Gérard et al.*, 2003], up to the extreme cases represented by the polar flares [*Waite et al.*, 2001], which can rise from the background level of a few kR to several megaRayleighs (MR) in brightness in tens of seconds. *Grodent et al.* [2003b] suggested that the polar emissions may be distributed over three regions fixed in magnetic local time (MLT): the dark region, a region devoid of emission appearing on the dawnside of the auroral region and associated with the return of previously emptied flux tubes; the swirl region, a region of faint patchy emission features appearing near the magnetic pole, likely associated with the region of open magnetic flux mapping to the tail lobes [*Cowley et al.*, 2003]; and the active region confined to the noon to dusk side, which contains the polar flares and is likely associated with the site of dayside magnetic reconnection of the Jovian magnetic field lines with the IMF.

[11] In addition to these general structures, secondary auroral features are frequently observed. A secondary oval, appearing equatorward of the main oval (Figure 1c), mainly at longitudes smaller than 180°, has been reported in several images [*Grodent et al.*, 2003a]. It may represent a first step in the process of corotation enforcement. Distinct patches of auroral emission often appear at all longitudes, between the main oval and the latitude of the Io trailing tail (Figure 1b). They suggest Earth-like injections of hot plasma in the inner magnetosphere [*Mauk et al.*, 2002], or bursty bulk flow processes [*Baumjohann et al.*, 1990; *Angelopoulos et al.*, 1994]. Dawn storms are spectacular features [e.g., *Gérard et al.*, 1994; *Ballester et al.*, 1996; *Clarke et al.*, 1998] which are characterized by a strong and localized brightening (in excess of 1 MR) in the dawn sector of the main oval, which resembles the feature highlighted in Figure 1b (see section 4). *Woch et al.* [2002] and *Cowley et al.* [2003] suggested that they may be associated with magnetic reconnection events in Jupiter's tail.

2.2. Nightside Polar Spots

[12] Figure 2 illustrates the temporal evolution of the morphology of the new feature, which we will refer to as nightside polar spots (NPS), in a series of images taken on 18 December 2000 (Figure 2a is a close-up view of Figure 1a). The ten images span a total time period of ~2500 s. In Figure 2a the NPS is made of two distinct spots that appear brighter than and poleward of the main oval. The faintest spot (marked 2) is poleward of the brightest one (marked 1). The second spot is undoubtedly completely detached from the main oval. Two minutes later (Figure 2b) the two spots are still present at the same location, although the brightness of spot 2 has decreased relative to spot 1 (brightness aspects will be discussed in the next sections). In Figure 2c, 5 minutes later, spot 2 has faded below the background level while spot 1 continues to brighten. The same situation prevails two minutes later (Figure 2d). After about 5 minutes, two new faint secondary spots (marked 2 and 3 in Figure 2e) have appeared to the left and right of spot 1. After two minutes (Figure 2f) spot 3 had disappeared. At this point, the brightness of spots 1 and 2 has started to decrease rapidly. In Figure 2g, five minutes later, spot 2 has almost disappeared, but after ~ eight minutes Figure 2h shows that spot 2 is still present. It should be noted that Figure 2h displays a time tagged image which was obtained with an additional filter, cutting most of the Ly-α emission, and integrated over the 300 s exposure time, so that the background level appears fainter than in Figure 2g. In Figures 2i and 2j, about ten minutes later, the two spots can hardly be discriminated from the main oval emission. In summary, the lifetime of spot 1 is at least 30 min. During this period the brightness

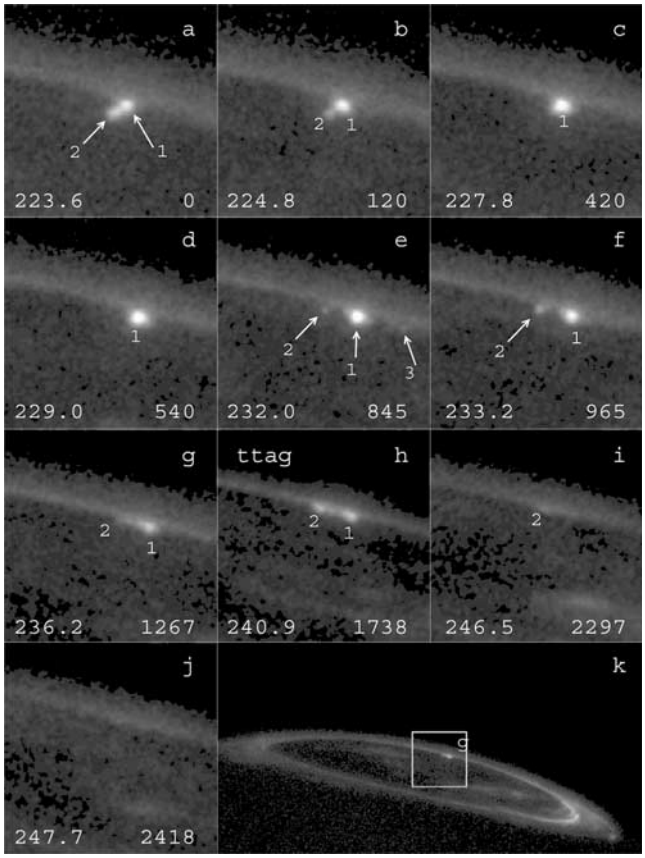

Figure 2. Evolution of the morphology of the NPS in the STIS data set obtained on 18 December 2000. Distinct spots are marked with ID numbers 1, 2, and 3. The number in the bottom left corner of each panel is the CML at mid-exposure, and the bottom right corner number gives the time spanned (in seconds) since the first image of the series (Figure 2a). The image displayed in Figure 2h was obtained in time tagged mode with an additional filter (see text). Figure 2k shows the limits of the zoomed sector appearing in Figure 2g.

of the spot increased and then decreased below the background level. Secondary spots appeared near spot 1 with lower brightnesses and shorter lifetimes.

3. Data Analysis

3.1. Location and Size of the Spots

[13] The first step in the analysis of the new auroral feature consists of finding the position of the spots in Jovicentric coordinates and their spatial extent on the planet surface. Previous studies [e.g., *Livengood et al.*, 1992; *Grodent et al.*, 1997; *Gérard et al.*, 1998] have demonstrated that the vertical extent of the auroral emission is of prime importance for the analysis of auroral structures appearing near the limb where geometrical effects, such as limb brightening, make it difficult to untangle the intrinsic characteristics of the auroral emission. The Chapman function gives the ratio of the slant column emission rate to the vertical column emission rate. However, this function is only appropriate for an emission uniformly covering the planet. This is clearly not the case for Jovian auroral emissions, which are generally organized in narrow arcs. Consequently, we have developed a simple numerical model which estimates the position, the size, and the limb brightening effect of a small spot appearing just below the Jovian limb.

[14] This procedure requires a model emission vertical profile. *Grodent et al.* [2001] used an energy degradation model from which they obtained two emission profiles meant to reproduce the emissions of a diffuse (unstructured emission) and a discrete aurora (arcs). This model considers an electron energy flux at the top of the Jovian atmosphere and self-consistently calculates the vertical temperature profile, the composition structure, and the degraded energy flux of the electrons as they penetrate deeper into the Jovian atmosphere. In this scheme, the principal input parameter is the energy spectrum of the precipitating electrons. It was adjusted to meet observational constraints such as the altitude of the H_2 emission peak, the thermal infrared and ultraviolet emissions, and the temperatures associated with various optical signatures. Here we consider the discrete auroral case, which is displayed in the top left corner of Figure 3. In order to obtain an analytical form for this profile, it is fitted with three Chapman profiles (dashed lines in Figure 3). The resulting emission profile $J(z)$ (dashed-dotted line in Figure 3) is given by equation (1), where H_i is the emission scale height, z_{0i} is the emission peak altitude, and w_i is the weight of each component in the sum. These parameters are listed in Table 1.

$$J(z) = \sum_{i=1}^{3} w_i I(H_i, z_{0i}) \quad \text{with} \quad I(H, z_0) = \alpha \exp(-\alpha) \quad \text{and}$$
$$\alpha = \exp\left(-\frac{(z - z_0)}{H}\right). \tag{1}$$

[15] The numerical model procedure that has been applied to the STIS images is threefold and gives rise, for each

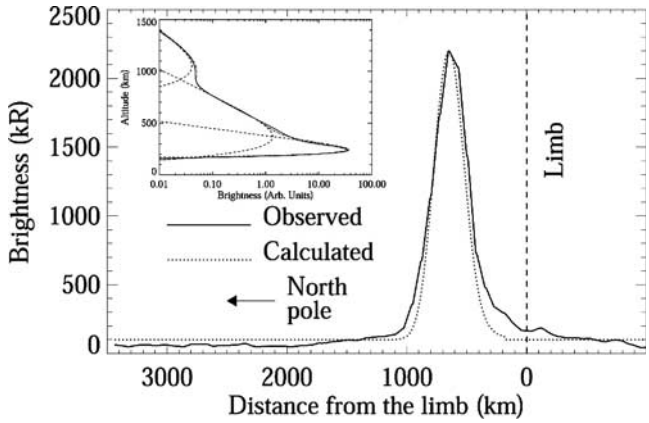

Figure 3. Illustration of the method used to determine the position and size of the emitting spots. The top left insert shows the vertical extent of the emission which was considered in the calculations (solid line, taken from *Grodent et al.* [2001]). The dashed lines represent the three Chapman profiles which were used to fit this emission profile. The solid line of the main plot is the emission distribution along a cut through Figure 2f, perpendicular to the limb. The dotted line was calculated using the vertical emission profile appearing in the insert, with the resulting distance and width listed in Table 2 (penultimate row).

Table 1. Characteristics of the Three Chapman Components Used in Equation (1) to Fit the Emission Profile Displayed in the Top Left Corner of Figure 3

Component	Scale Height, km	Emission Peak Altitude, km	Weight %
1	30	240	96.32
2	110	370	3.57
3	150	1050	0.11

image, to a plot similar to that illustrated in Figure 3. (1) The limb of the planet is determined with the procedure described by *Grodent et al.* [2003a] (the error caused by the inaccuracy of the limb fitting procedure will be discussed in the next section). (2) A cut perpendicular to the limb, passing through the maximum of the spot is extracted from the image. The emission distribution along this profile is fitted with a Gaussian distribution plus a constant term which represents the background baseline emission. The distance from the limb is assumed to be the distance between the limb and the peak of the Gaussian fit. The Gaussian is then deconvolved by the instrumental PSF using 8 iterations of the maximum likelihood method, where the PSF is defined by a Gaussian distribution with a FWHM of 200 km (2.8 pixels). (3) The distance from the limb and the PSF corrected width are injected in a grid-search code which uses equation (1) to estimate the width and the center position of the emission region on the planet surface (i.e., the 1-bar pressure level) which, after integration along the line of sight, gives rise to the spot observed under grazing incidence. In this last step the emission region is assumed to be isotropically emitting. Figure 3 compares the resulting calculated emission profile, accumulated along the line of sight and back convolved by the PSF, with the observed spot 1 appearing in Figure 2f.

[16] Table 2 lists the center position and size of the emission regions in Jovicentric coordinates. Five spots were considered on 14 December 2000, four spots on 16 December 2000, and seven on 18 December 2000. The latter spots correspond to spot 1 in Figures 2a–2g. As expected from the accumulation of emission along the line of sight, the brightening factor given in the last column is proportional to the spatial extent of the emission region. It is also inversely proportional to the distance from the limb and varies from ~5 to 10. The Jovicentric latitudes are noticeably concentrated in a small range centered on 72.4°, while the longitudes, around 161°, increase with the CML. It is instructive to note that in the 18 December 2000 sequence, where the same spot could be followed for up to 30 min, the longitude variation of the emission spot is about 70% of the CML variation, meaning that the emitting region is not corotating with the magnetic field but is not fixed in local time either. As a result of the asymmetry of the Jovian magnetic field, if a plasma parcel in the magnetic equator were fixed relative to the direction of the Sun, then its magnetic footprint in the ionosphere would be said to be fixed in MLT and move in latitude and longitude at a rate different from the corotating auroral features. We have applied the magnetic model described by *Khurana* [1997] to a plasma parcel associated with the region where the spots appear when the CML is close to 220° (the notion of magnetic mapping will be discussed in section 3.4). It appears that the longitudinal velocity of a MLT fixed auroral footprint in this region is about 40% of the velocity of a point fixed on the planet surface. Therefore the longitude increase of the emission spot observed in the 18 December 2000 sequence (70%) is just between the case of an auroral feature fixed in MLT (40%) and the case of a corotating feature (100%).

3.2. Sensitivity Study

[17] *Grodent et al.* [2003a] have shown that the inaccuracy of the limb fitting procedure leads to an imprecision in the location of large scale emission regions which, near the

Table 2. Position and Size of the Spots[a]

Date	Spot	CML (S3°)	Apparent Distance,[b] km	Apparent Width,[c] km	Longitude (S3°)	Jovicentric Latitude, deg	ALT, hours	Surface Width,[d] deg	Brightening Factor
14 Dec. 2000	br	209.4	761	331	145	72.6	20.3	4.3	6.8
	fa	210.6	710	266	146	72.7	20.4	3.5	6.7
	br	210.6	1117	63	154	73.6	20.4	0.7	4.5
	br	214.1	924	91	156	73.9	20.7	1.0	5.0
	fa	214.1	515	265	146	72.6	20.6	3.9	7.7
16 Dec. 2000	br	220.1	1112	97	161	71.4	19.6	1.0	4.7
	br	221.3	1072	99	162	71.5	19.7	1.1	4.8
	br	243.0	211	232	173	73.1	21.1	3.9	9.7
	br	244.2	205	233	175	73.0	20.8	3.9	9.7
18 Dec. 2000	a1	223.6	875	155	162	71.8	19.9	1.8	5.6
	b1	224.8	837	121	162	71.9	20.1	1.4	5.5
	c1	227.8	780	134	165	71.9	20.0	1.7	5.7
	d1	229.0	768	130	166	72.0	20.1	1.6	5.7
	e1	232.0	681	116	168	72.0	20.1	1.5	5.9
	f1	233.2	632	123	169	72.0	20.0	1.6	6.1
	g1	236.2	539	121	171	72.1	20.0	1.7	6.5

[a]In the case of multiple spots, the two-letter code "br" (second column) refers to a bright spot, and "fa" refers to a faint spot for the 18 December 2000 data set; the letter refers to the panel of Figure 2, and the digit refers to the spot number in this panel. The ALT is the auroral local time, in hours, defined in Appendix A.

[b]Apparent distance measured from the limb in the direction perpendicular to the limb.

[c]Apparent Gaussian width of a spot after deconvolution by the PSF, measured in the direction perpendicular to the limb.

[d]Calculated surface width of the emitting region (different from the apparent width), 1° corresponds to ~1200 km on the surface.

Table 3. Sensitivity Tests Performed With a Simplified Emission Profile Consisting of a Single Chapman Profile[a]

z_0, km	H, km	Distance, km	Width, deg	Latitude, deg
240	100	600	1.8	72.0
200	100	600	1.8	71.8
280	100	600	1.7	72.2
240	**50**	600	2.0	71.9
240	**150**	600	0.7	72.0
240	100	**400**	2.0	70.9
240	100	**800**	1.6	75.0

[a]The emission peak altitude and scale height are given in the first two columns. The table lists the effects of varying the emission peak altitude z_0, the scale height H, and the distance from the limb on the calculated surface width (column 4) and latitude of the center of the emitting surface (column 5). The numbers in bold are the parameters that have been varied. The first row corresponds to the reference case.

limb, may be more than 5° in longitude and/or latitude. However, this estimate was based on an image projection procedure which assumed that all the emission is concentrated in an infinitely thin layer 240 km above the 1 bar pressure level, in other words neglecting the full vertical extent of the auroral emission. The estimate of the position inaccuracy for the vertical emission of a spatially limited feature just below the limb, seen under grazing incidence, requires a more specific treatment. Accordingly, the method described in the above section was used to estimate the effects of varying different parameters on a typical test case. For simplicity, the emission profile given by equation (1) was replaced by a single Chapman profile. Table 3 lists the sensitivity of the surface width and latitude of the emission region to the altitude of the emission peak, to the emission scale height, and to the measured distance from the limb. The emission peak altitude was varied by ±40 km (*Vasavada et al.* [1999] derived an emission peak of 245 ± 30 km). It results in a small change in latitude of ±0.2°. Varying the emission scale height from 50 to 150 km (a drastic change) influences the surface width of the emission region by up to a factor of 3. Finally, an error made on the distance from the limb of ± the size of the PSF (200 km) has a major effect on the latitude which varies from +3 to −1° from its nominal value. In order to estimate the effect of varying the distance from the limb on the longitude, we have considered the penultimate case listed in Table 2. A ±200 km variation of the distance from the limb gives rise to a ±3° variation of the longitude and ∓0.4° of the latitude. In summary, this sensitivity analysis shows that a rather large uncertainty on the measured distance from the limb on the order of ± the size of the PSF gives rise to error bars of +3/−1° in latitude and ±3° in longitude. The width of the emission region is mainly influenced by the emission scale height, i.e., the vertical extent of the emission profile, and can more than double in extreme cases.

3.3. Brightness

[18] Once the position of the spot is known, the level of limb brightening (last column of Table 2) and the geometrically corrected brightness may be evaluated to determine the vertical brightness. Figure 4 shows the variation of the maximum brightness in kR above the background, corrected for the view angle, as a function of time for the series of images taken on 18 December 2000. The letters a to g refer to spot 1 in the corresponding panels in Figure 2. The maximum brightness of spot 1 was sampled for 21 min in seven ∼100 s bins. During the first 850 s, the brightness continuously increased from 280 kR to 485 kR. It then abruptly decreased during the next 450 s dropping to a value of 150 kR above the background emission. The dashed lines in Figure 4 are best fit functions passing through the data points. During the brightness rising phase, the data points are well adjusted on a $(1 - \exp(-t/\tau_r))$ function, where t is the time and τ_r is the characteristic rise time equal to 370 s. The decreasing phase is fit with a $(\exp(-t/\tau_d))$ function, where τ_d is the characteristic decrease time equal to 213 s. It is interesting to note that this behavior is analogous to that of the current flowing through a RL electric circuit during the charge and discharge phases of the inductor, as magnetic energy is stored then suddenly released. The difference in characteristic time would then be attributed to a modification of the resistance and/or the inductance of the circuit. Without going too far in this simple analogy, it should be at least mentioned that the relationship between brightness and such current I is not straightforward. The brightness is likely a complex function of I and/or I^2. In the linear case, the characteristic times of brightness and current are the same, while in the quadratic case the exponential trend is preserved, and the rise and decrease times of I are twice larger than those of the brightness.

[19] The brightness uncertainty applicable to Figure 4 has two distinct origins: the first one is instrumental and is estimated from the square root of the count number (assuming Poisson statistics) which leads to a value ranging from ±10% for the faintest points (mostly g) to ±4% for the brightest ones (c, d, e). The second source is tied to the modeling of the absolute brightness of the spots. It consists of a ±10% uncertainty related to the conversion from counts to emitted H_2 kR, and of a ±5% inaccuracy resulting from

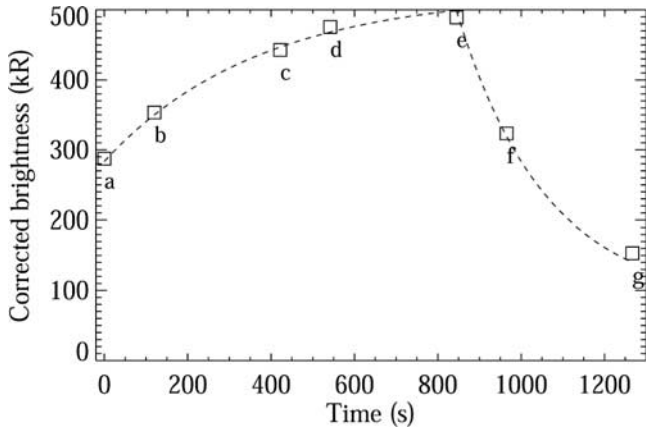

Figure 4. Evolution of the maximum brightness, corrected for the viewing angle, of spot 1 appearing in Figures 2a–2g. The dashed line was obtained by fitting a $(1 - \exp(-t/\tau_r))$ function for the rising phase and a $(\exp(-t/\tau_d))$ function for the decreasing phase. The characteristic times are $\tau_r = 370$ s and $\tau_d = 213$ s, respectively. See text for a discussion on the brightness uncertainty.

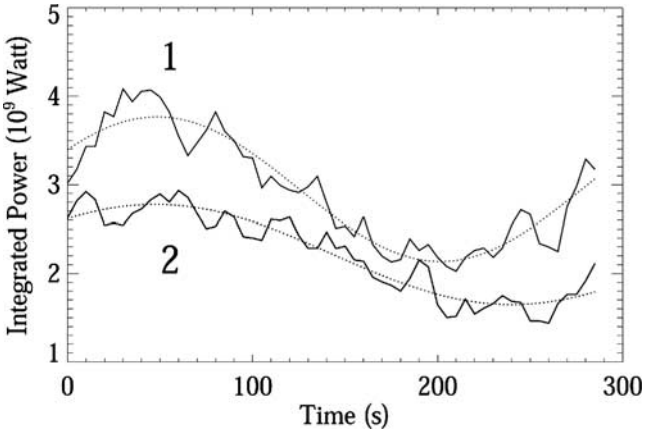

Figure 5. Integrated power emitted by spot 1 (top line) and spot 2 (bottom line) of Figure 2h as a function of time. These light curves were derived from a time tagged image with 5-s sampling bins, smoothed over 15 s with a boxcar average. The dotted curves were obtained by fitting a function of the form ($A \sin(2\pi t/\tau_s + \phi)$) (see text). For spot 1 the characteristic time (or period) is 306 s, and it is 385 s for spot 2.

the propagation of the 200 km positional uncertainty on the brightening factor (last column of Table 2). However, the latter error source is systematic and affects all the points by the same amount, so that it has no effect on the trend presented in Figure 4.

[20] If one assumes that a downward beam of electrons carrying 1 mW m^{-2} is necessary to produce 10 kR of H_2 far-UV emission [*Grodent et al.*, 2001], then an energy flux of ~15 to 50 mW m^{-2} is needed to produce the observed emission. Unfortunately, no spectral information on the observed spots is available so that it is impossible to infer the mean energy of the primary electrons which may have produced this emission [*Gérard et al.*, 2003]. However, as already noted, the image appearing in Figure 2h was taken in time tag mode with an additional filter blocking the strong Ly-α emission line. This emission line is sensitive to the level of hydrocarbon absorption and, by comparing it with unabsorbed emission lines, it can be used as a marker for the penetration depth of the electron beam and therefore of its mean energy. In our case, the brightness levels of filtered and unfiltered images were comparable. This means that the level of absorption was not uncommonly strong, at most typical of electrons having a mean energy of a few tens of keV. However, it should be noted that the filtered/unfiltered images were not taken simultaneously, whereas Figures 4 and 5 show strong temporal emission variations. Figure 5 shows the temporal evolution of the power of spots 1 and 2 in Figure 2h. The light-curves are given in units of emitted power integrated over the spot area, after background subtraction. The time tagged image was sampled in 5-s bins and the solid curves were additionally smoothed over 15 s with a boxcar average. The emitted power varies from ~1.5 to 4 $\times$ 10^9 W. For a circular surface emission region of 2.5 $\times$ 10^6 km^2, assuming a conversion efficiency of emitted/injected power of 10%, this integrated power range corresponds to an injected energy flux of ~6 to 6 mW m^{-2}, in agreement with the previous estimate. The most prominent fact of Figure 5 is the sinusoidal variation of the light-curves. The dotted curves were obtained by fitting a function of the form ($A \sin(2\pi t/\tau_s + \phi)$), where A is the amplitude, τ_s is the period and ϕ the phase angle. For spot 1 (top curve) $A = 8.2 \times 10^8$ W, $\tau_s = 306$ s and $\phi = 33°$, and for spot 2 (bottom curve) $A = 5.6 \times 10^8$ W, $\tau_s = 385$ s and $\phi = 45°$. These numbers suggest that the total power emitted by the two spots varied in parallel for at least one full sinusoidal period of ~300 s. The amplitude of the oscillation was about 20% of the average emitted power, more than twice the σ value associated with the Poisson photon counting statistics.

3.4. Magnetic Mapping of the Spots

[21] In this final step of the image analysis, we address the location of the magnetospheric region responsible for auroral spots. Although their size and brightness are comparable to that of the Io footprint, a search of the Io, Ganymede and Europa satellites' orbital positions and projected magnetic footprints (using the VIP4 magnetic model [*Connerney et al.*, 1998]) shows that none of them matches the position of the spots given in Table 2. Actually, this is straightforward for the Io footprint which appears in the three panels of Figure 1. As already noted, the spots are located poleward of the main auroral oval. This indicates that they actually originate from a distant region of the magnetosphere, probably farther than 30 R_J. A more precise mapping of the auroral emission features requires a magnetic model able to trace a magnetic field line from the Jovian ionosphere out to the distant magnetosphere. Although the VIP4 magnetic model has been widely used for this purpose, it was not meant to be accurate beyond ~25–30 R_J. At these distances other models which include the effect of the current sheet may be used to estimate the local field. Therefore we have used the magnetospheric model developed by *Khurana* [1997]. It combines the internal magnetic field used in the VIP4 model, i.e., the GSFC-O_6 model, and models of the external field arising from the various current sources present in the magnetosphere. This choice was mainly dictated by the fact that Khurana's 1997 model is applicable to the middle and outer nightside magnetosphere.

[22] Table 2 shows that the latitude of the spots is almost constant at ~72°, while their longitude varies with the CML. According to Khurana's 1997 model, and accounting for the deviation of the main oval along the 150° meridian (the kink sector of *Grodent et al.* [2003a]), the 150–160° longitude range, seen at CML $\simeq$ 230° maps to a region of the magnetosphere beyond 100 R_J around 2100LT in the night sector. It should be noted that at these distances, Khurana's 1997 model does not account for the magnetopause currents which produce local time asymmetries. More specifically, the solar wind driven magnetopause-tail current system will likely stretch the field lines further away from noon [*Bunce and Cowley*, 2001]. This latter effect would thus shift the magnetospheric end of the field lines toward higher local times and larger distances. Accordingly, the location of the source region beyond 100 R_J around 2100LT may be seen as a rough estimate.

[23] An alternative to the magnetic local time obtained from the VIP4 model is described in Appendix A. We have defined an "auroral clock" which gives the auroral local time (ALT) of any feature in the northern auroral region.

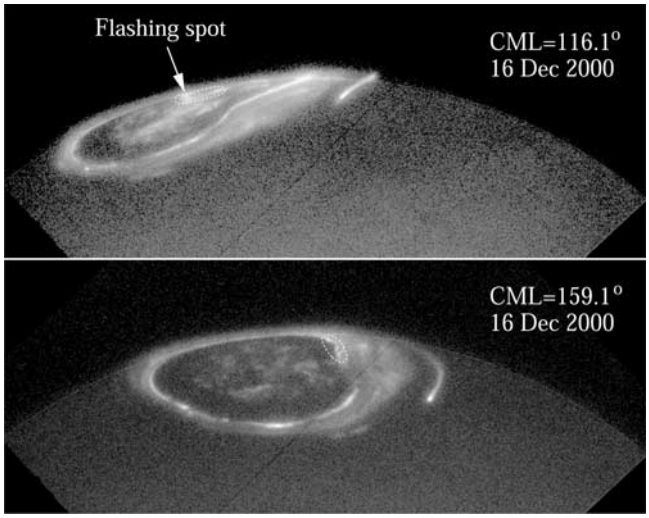

Figure 6. HST-STIS images of the northern auroral region of Jupiter obtained on 16 December 2000 at two different CMLs. The emission spots enclosed in the dotted contours ("flashing spot" for the top panel) are magnetically mapped to the premidnight tail region, beyond 100 R_J, and may therefore represent possible NPS signatures, similar to those observed at CML close to 220° in Figure 1. See color version of this figure at back of this issue.

The main advantage of this simplified local time system is that it accounts for the variations of the complex auroral morphology with the CML (actually with the subsolar longitude), but is not contingent upon any magnetic field model. The main limitation of the ALT is that it does not provide the distance to which the auroral feature is mapping. Since the field line bending is no longer accounted for, one might expect differences of ±1 hour, depending on the distance, with the MLT time derived with VIP4 in the same CML range. The ALT of the nightside polar spots are given in Table 2. It appears that each spot is characterized by a time ranging from 1936ALT to 2106ALT.

[24] Keeping the limitations of the VIP4 mapping in mind, one might estimate the size of the magnetospheric source region by noting that, at 100 R_J, a 1° change in longitude corresponds to a 5 to 10 R_J change in location at the magnetic equator. Therefore a spot characterized by a surface width ranging from 1° to 4.3° (Table 2) would magnetically map to a region having a characteristic size of ∼5 to 50 R_J. The important focussing of the magnetic field lines, from the magnetosphere toward the ionosphere, may therefore explain the very small appearance of the spots.

[25] In the case of a magnetospheric source region fixed in local time, the spots should appear at different locations as the CML changes. According to Khurana's 1997 model, the nightside source region should give rise to emission spots which, when seen at CML ≃ 120°, would appear near longitude 220°, that is just at the limb, at a latitude close to 75°. This location corresponds to midnight ALT, that is later than 2100ALT deduced from the spots appearing when CML ∼ 220°. This time lead stems from differences between the MLT and ALT systems (see Appendix A) and/or from a variation of the location of the magnetospheric source region. The top panel of Figure 6 displays an image taken on 16 December 2000 at CML = 116.1°. Interestingly, a series of spots appear between longitude 190°–210°, and latitude 70°–80° (dashed contour). One of them (marked with an arrow) appeared to flash once, as its brightness more than doubled in 6 min. This image is the third in a 6-image sequence spanning ∼17 min. The spots were clearly visible in the four first images, then faded away in the last two images. At CML ≃ 160°, Khurana's model predicts that the same source region, at 2100ALT in the magnetosphere, maps to the 130°–150° longitude range, and 80°–90° latitude range. The image displayed in the bottom panel of Figure 6 was taken on 16 December 2000 at CML = 159.1° and shows three distinct spots in the expected range (dashed contour). It should be noted that the discontinuous temporal distribution of the imaging sequences of the auroral emission prevents us from asserting that the spots observed in Figures 1b and 6 are related to the same process.

3.5. Other Occurrences of the Spots

[26] So far, we have discussed the case of images clearly showing emission spots at the limb on 14, 16, and 18 December 2000. On the other days of the present observation campaign (28 December 2000, 13, 20, and 21 January 2001) the identification of such auroral features is more ambiguous. On 28 December 2000, no image of the northern hemisphere was taken at a CML close to 220°. On 13 January 2001, two images were taken at a CML = 218.7° and 242.4°. They show a localized brightening of the emission appearing at the limb, close to the expected location, but no distinct spots were detected (a case similar to that illustrated in Figures 2i and 2j where the emission spots had almost disappeared). The same morphology prevails on 20 January 2001, when 10 images were taken in the appropriate CML range. On 21 January 2001, one image was taken at CML = 207.1° which shows a faint emission spot, slightly poleward of the main oval.

[27] As far as the NPS is concerned, the images resulting from a search through the STIS data set, back to 1997, are similar to the 13 to 21 January 2001 images. On the 10 images taken at a CML in the range 200–250° only two of them show faint, distinct emission spots poleward of the main oval, near latitude 70–75°. The other eight images just showed a brightening similar to that observed in Figure 2j. Therefore it may be concluded that the brightness and the poleward location of the isolated spots that have been observed on 14, 16, and 18 December 2000 were relatively unusual.

4. Summary and Discussion

[28] Although there are many in situ clues suggesting reconnection processes in the Jovian magnetotail, to date only *Woch et al.* [2002] and *Cowley et al.* [2003] have suggested that they should give rise to a specific auroral signature. In this paper, we report the observation of a new auroral feature, forming isolated spots near the northern dusk-midnight limb, poleward of the main auroral oval, which we consider to be a possible auroral signature of magnetotail reconnection activity at Jupiter. This unusual feature was clearly detected in three HST-STIS data sets obtained on the 14, 16, and 18 of December 2000, but not

Table 4. Comparison of the Characteristics of the in Situ Reconnection Events With Those Derived From the Auroral Emission Spots[a]

	In Situ	Auroral Spots
Distance	>50 R_J (70–120 R_J)	>100 R_J
Location	postmidnight	premidnight
Char. size	25 R_J	5–50 R_J
Duration	minutes to few hours	5 minutes to 1 hour
Recurrence	4 hours to 1 day, 2–3 days	most of the time to 1–2 days

[a]The in situ characteristics are discussed in section 1 and were obtained from *Russell et al.* [1998, 2000] and *Woch et al.* [1999, 2002].

on the four other days of the present observing campaign. In earlier STIS data sets, back to 1997, only two out of ten images taken in the 200–250° CML range show similar but much fainter distinct emission spots poleward of the main oval. Most of the other images just show a localized brightening or more diffuse features in the region of interest.

[29] The principal characteristics derived from the auroral spots are summarized in Table 4. They are compared with those events in the night side magnetosphere that were observed by in situ spacecraft (mainly Galileo) which were associated with reconnection and substorm-like events. The in situ events are generally found beyond 50 R_J, more precisely between 70 and 120 R_J in the postmidnight sector. However, it should be emphasized that the premidnight dusk sector was poorly covered by Galileo, and the concentration of the events in the postmidnight sector could, in part, stem from a spacecraft orbital selection effect. The mapped magnetospheric origin of the auroral spots appears to be located beyond 100 R_J in the premidnight sector. This mapping rests on *Khurana*'s [1997] magnetic model, which does not account for magnetopause currents that would likely stretch the field lines, and the origin of the auroral spots, further away in the anti-sunward direction, i.e., closer to midnight. The characteristic size of the reconnection site has been estimated to be 25 R_J, consistent with the 5–50 R_J range deduced from the size of the auroral spots. The duration of the reconnection events has been shown to range from several minutes to a few hours. This is compatible with the characteristic time of the auroral brightness fluctuations of ~5 minutes, and the occurrence of the spots in image sequences spanning about an hour. Small reconnection events are found to recur irregularly every ~4 hours and large events once a day, while important particle bursts appear every 2–3 days. In the present observation campaign, the brightest auroral spots are observed over a 5-day period with a 1-day gap, while faint localized brightenings appeared on most of the images taken during the other days of the campaign. In conclusion, the similarities between the characteristics of the reconnection site and those inferred from the auroral spots support the idea that the emission spots are an auroral signature of reconnection events taking place in the distant Jovian magnetotail.

[30] In addition to the characteristics listed in Table 4, it may be stated that the measured spot brightnesses ranged from 170 to 510 kR of H_2 emission (after correction for the viewing geometry), corresponding to an input energy flux of 17–51 mW m^{-2} and a total injected power of 15–40 GW. On one day, the spots were shown to rotate at 70% of the rigid corotation velocity. According to Khurana's magnetic model, this feature, when seen at a CML close to 220°, is magnetically connected to a magnetospheric plasma parcel moving at ~50% the corotation velocity. In many regards the morphology and the dynamics of the NPS are similar to that of the pseudo-dawn storm highlighted in Figure 1b. *Grodent et al.* [2003a] named this latter feature Multiple Dawn Arcs (MDA) because it appears different from the dawn storms which have been described in the literature [e.g., *Gérard et al.*, 1994; *Ballester et al.*, 1996]. It shares some characteristics with the substorm spots: it is located poleward of the main oval and maps to the nightside magnetosphere, it consists of two to three small separate structures in near-rigid corotation. On 16 December 2000, the NPS and the MDA appeared on the same images, meaning that they may have been triggered by similar magnetospheric events which took place at different times and/or locations.

[31] As pointed out by *Grodent et al.* [2003a] and *Cowley et al.* [2003], the association of an auroral feature with reconnection across the night side current sheet implies that this auroral emission is located on closed, near-corotating field lines downstream of the reconnection site. The near-rigid corotation (~50%) of the closed field lines, after reconnection, may thus stem from the loss of plasma mass which was carried away by the released plasmoid. The auroral emissions observed at the feet of the newly closed field lines could then be related both to precipitation of plasma heated in the reconnection process, and to the field-aligned currents that couple the changing angular momentum of the flux tubes between the magnetosphere and the ionosphere. Yet another likely candidate is the Birkeland current associated with interchange convection cells.

[32] The common factor between the auroral processes at Earth and Jupiter is magnetotail reconnection and its auroral counterpart in the planetary atmosphere. However, the cause of this sporadic reconnection differs from object to object. For example in the case of Earth, the cause is the overloading of magnetic energy in the tail due to day side reconnection with the IMF (the "substorm process"), whereas in the solar corona, the cause is the overloading of plasma thermal energy in coronal magnetic loops (the "coronal mass ejection" or CME). In the case of Jupiter, it is the overloading of plasma thermal and rotational energy in the tail due to iogenic mass loading (the "planetary wind" process). The Jovian case is, if anything, more nearly analogous to the solar case than to the terrestrial case. The NPS which have been described in this work may therefore be associated with the process of "magnetotail reconnection" which is closely related to "Jovian mass ejection," analogous to the solar CME process.

Appendix A

[33] The auroral local time (ALT) system provides a convenient way to approach the magnetic local time (MLT) in the northern hemisphere, without any reference to a magnetic model. The ALT time is calculated from the α and α_S angles, and from the β and β_S arc lengths displayed in Figure A1. It gives local times in Jovian hours, where 24 Jovian hours represent ~9.9 Earth hours. In this auroral coordinate system, α may be seen as an azimuth angle around the auroral pole, measured clockwise from the spin

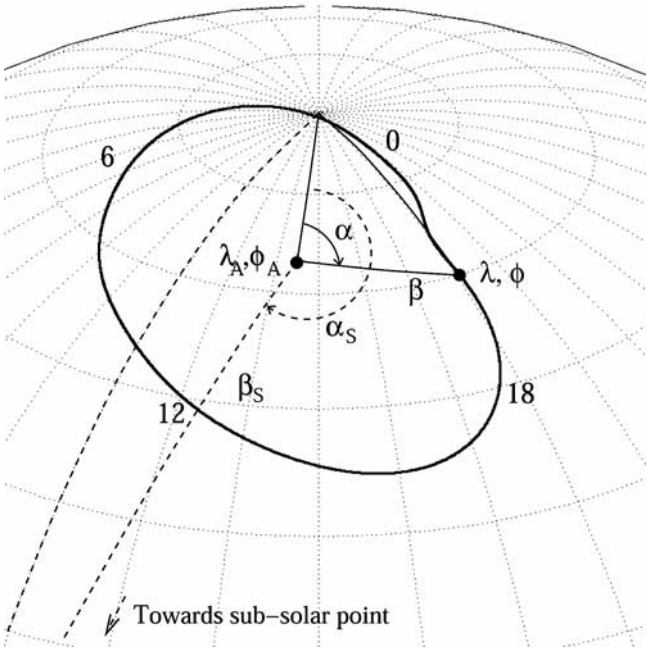

Figure A1. Illustration of the auroral local time (ALT) system. The ALT of an auroral feature characterized by a longitude λ and a latitude ϕ is calculated from the "center" of the main auroral oval, at a position λ_A, ϕ_A, and from the position of the subsolar point given by λ_S and ϕ_S. A 10° spaced grid is overplotted, and the tilt of the planet is set to 30° for clarity. The subsolar point, near the equator, appears out of the figure. The formulae calculating α, β, α_S, and β_S are given in Appendix A.

pole, and β as an auroral co-latitude, measured from the auroral pole. They are calculated with the following spherical trigonometric relations:

$$\beta = \arccos\{\sin\phi\,\sin\phi_A + \cos\phi\,\cos\phi_A\,\cos(\lambda_A - \lambda)\}, \quad \text{(A1)}$$

$$\alpha = \arctan\left\{\frac{\cos\phi\,\cos\phi_A\,\sin(\lambda_A - \lambda)}{\sin\phi - \sin\phi_A\,\cos\beta}\right\}, \quad \text{(A2)}$$

where λ and ϕ are the longitude (S_{III}) and latitude (Jovicentric), respectively, of the auroral feature for which we calculate the ALT; λ_A and ϕ_A are the longitude and latitude of the auroral pole. The same expressions hold for β_S and α_S when λ_S and ϕ_S (the longitude and latitude of the subsolar point) are substituted for λ and ϕ. Finally, the ALT is given by

$$ALT = 12 - \frac{\alpha - \alpha_S}{15}, \quad \text{(A3)}$$

where α and α_S are in degrees.

[34] In Table 2, we have assumed that the auroral pole corresponds to the "center" position of the main oval which we have set to $\lambda_A = 185°$ and $\phi_A = 74°$. The estimation of this position is somewhat arbitrary. For example, different values are obtained if the center is deduced from an orthographic polar projection of the main oval or from an azimuthal equidistant polar projection. However, in this example the values are very close. In the case of the first row of Table 2, varying ϕ_A by ±2° leads to a variation of ALT of ∓40 minutes, and a variation of λ_A of ±10° gives rise to a change of ALT on the order of ∓15 minutes. Accordingly, the accuracy of the ALT "clock" is on the order of ±1 hour, and it may be adjusted by shifting the center position corresponding to the auroral pole. A comparison of the ALT and MLT times, using the VIP4 model, shows that at 15 R_J, i.e., the orbit of Ganymede, the ALT clock leads the MLT clock by a maximum value of ~2 hours for an auroral feature located near $\lambda = 190°$. It lags the MLT clock by maximum ~50 minutes at $\lambda \sim 135°$ and $\lambda \sim 245°$. At $\lambda \sim 0°$ the MLT and the ALT are almost the same.

[35] **Acknowledgments.** The authors would like to thank K. Khurana who provided us with his magnetospheric model. The authors also thank two anonymous referees for their valuable comments and suggestions. This work is based on observations with the NASA/ESA Hubble Space Telescope, obtained at the Space Telescope Science Institute (STScI), which is operated by AURA, inc. for NASA under contract NAS5-26555. DG and JCG are supported by the Belgian Fund for Scientific Research (FNRS). Partial funding for this research was provided by the PRODEX program of the European Space Agency (ESA).

[36] Arthur Richmond thanks the reviewers for their assistance in evaluating this paper.

References

Angelopoulos, V., C. F. Kennel, F. V. Coroniti, R. Pellat, M. G. Kivelson, R. J. Walker, C. T. Russell, W. Baumjohann, W. C. Feldman, and J. T. Gosling (1994), Statistical characteristics of bursty bulk flow events, *J. Geophys. Res.*, *99*, 21,257–21,280.

Ballester, G. E., et al. (1996), Time-resolved observations of Jupiter's far-ultraviolet aurora, *Science*, *274*, 409–412.

Baumjohann, W., G. Paschmann, and H. Lhr (1990), Characteristics of high-speed ion flows in the plasma sheet, *J. Geophys. Res.*, *95*, 3801–3809.

Bunce, E. J., and S. W. H. Cowley (2001), Divergence of the equatorial current in the dawn sector of Jupiter's magnetosphere, *Planet. Space Sci.*, *49*, 1089–1113.

Carbary, J. F., T. W. Hill, and A. J. Dessler (1976), Planetary spin period acceleration of particles in the Jovian magnetosphere, *J. Geophys. Res.*, *81*, 5189–5195.

Clarke, J. T., et al. (1998), Hubble Space Telescope imaging of Jupiter's UV aurora during the Galileo orbiter mission, *J. Geophys. Res.*, *103*, 20,217–20,236.

Clarke, J. T., et al. (2002), Ultraviolet auroral emissions from the magnetic footprints of Io, Ganymede, and Europa on Jupiter, *Nature*, *415*, 997–1000.

Connerney, J. E. P., M. H. Acuña, N. F. Ness, and T. Satoh (1998), New models of Jupiter's magnetic field constrained by the Io flux tube footprint, *J. Geophys. Res.*, *103*, 11,929–11,939.

Cowley, S. W. H., E. J. Bunce, T. S. Stallard, and S. Miller (2003), Jupiter's polar ionospheric flows: Theoretical interpretation, *Geophys. Res. Lett.*, *30*(5), 1220, doi:10.1029/2002GL016030.

Gérard, J.-C., D. Grodent, R. Prangé, J. H. Waite, G. R. Gladstone, V. Dols, F. Paresce, A. Storrs, L. Ben Jaffel, and K. A. Franke (1994), A remarkable auroral event on Jupiter observed in the ultraviolet with the Hubble Space Telescope, *Science*, *266*, 1675–1678.

Gérard, J.-C., D. Grodent, V. Dols, and J. H. Waite Jr. (1998), The longitudinal variation of the color ratio of the Jovian ultraviolet aurora: A geometric effect?, *Geophys. Res. Lett.*, *25*(10), 1601–1604.

Gérard, J.-C., J. Gustin, D. Grodent, J. T. Clarke, and A. Grard (2003), Spectral observations of transient features in the FUV Jovian polar aurora, *J. Geophys. Res.*, *108*(A8), 1319, doi:10.1029/2003JA009901.

Grodent, D., G. R. Gladstone, J.-C. Gérard, V. Dols, and J. H. Waite (1997), Simulation of the morphology of the Jovian UV north aurora observed with the Hubble Space Telescope, *Icarus*, *128*, 306–321.

Grodent, D., J. H. Waite Jr., and J.-C. Gérard (2001), A self-consistent model of the Jovian auroral thermal structure, *J. Geophys. Res.*, *106*, 12,933–12,952.

Grodent, D., J. T. Clarke, J. Kim, J. H. Waite Jr., and S. W. H. Cowley (2003a), Jupiter's main auroral oval observed with HST-STIS, *J. Geophys. Res.*, *108*(A11), 1389, doi:10.1029/2003JA009921.

Grodent, D., J. T. Clarke, J. H. Waite Jr., S. W. H. Cowley, J.-C. Gérard, and J. Kim (2003b), Jupiter's polar auroral emissions, *J. Geophys. Res.*, *108*(A10), 1366, doi:10.1029/2003JA010017.

Hill, T. W. (2001), The Jovian auroral oval, *J. Geophys. Res.*, *106*, 8101–8107.

Khurana, K. (1997), Euler potential models of Jupiter's magnetospheric field, *J. Geophys. Res.*, *102*(A6), 11,295–11,306.

Livengood, T. A., H. W. Moos, G. E. Ballester, and R. Prangé (1992), Jovian ultraviolet auroral activity, 1981–1991, *Icarus*, *97*, 26–45.

Louarn, P., A. Roux, S. Perraut, W. S. Kurth, and D. A. Gurnett (1998), A study of the large-scale dynamics of the Jovian magnetosphere using the Galileo Plasma Wave Experiment, *Geophys. Res. Lett.*, *25*, 2905–2908.

Louarn, P., A. Roux, S. Perraut, W. S. Kurth, and D. A. Gurnett (2000), A study of the Jovian "energetic magnetospheric events" observed by Galileo: Role in the radial plasma transport, *J. Geophys. Res.*, *105*, 13,073–13,088.

Mauk, B. H., J. T. Clarke, D. Grodent, J. H. Waite Jr., C. P. Paranicas, and D. J. Williams (2002), Transient aurora on Jupiter from injections of magnetospheric electrons, *Nature*, *415*, 1003–1005.

Nishida, A. (1983), Reconnection in the Jovian magnetosphere, *Geophys. Res. Lett.*, *10*, 451–454.

Paranicas, C. P., B. H. Mauk, and S. M. Krimigis (1991), Pressure anisotropy and radial stress balance in the Jovian neutral sheet, *J. Geophys. Res.*, *96*, 21,135–21,140.

Prangé, R., I. M. Engle, J. T. Clarke, M. Dunlop, G. E. Ballester, W. H. Ip, S. Maurice, and J. Trauger (1995), Auroral signature of comet Shoemaker-Levy 9 in the Jovian magnetosphere, *Science*, *267*, 1317–1320.

Russell, C. T., K. K. Khurana, D. E. Huddleston, and M. G. Kivelson (1998), Localized reconnection in the near Jovian magnetotail, *Science*, *280*, 1061–1064.

Russell, C. T., K. K. Khurana, M. G. Kivelson, and D. E. Huddleston (2000), Substorms at Jupiter: Galileo observations of transient reconnection in the near tail, *Adv. Space Sci.*, *26*(10), 1499–1504.

Satoh, T., J. E. P. Connerney, and R. L. Baron (1996), Emission source model of Jupiter H_3^+ aurorae: A generalized inverse analysis of images, *Icarus*, *122*, 1–23.

Stallard, T. S., S. Miller, S. W. H. Cowley, and E. J. Bunce (2003), Jupiter's polar ionospheric flows: Measured intensity and velocity variations poleward of the main oval, *Geophys. Res. Lett.*, 30, 1221, doi:10.1029/2002GL016031.

Vasavada, A. R., A. H. Bouchez, A. P. Ingersoll, B. Little, C. D. Anger, and the Galileo SSI Team (1999), Jupiter's visible aurora and Io footprint, *J. Geophys. Res.*, *104*, 27,133–27,142.

Vasyliūnas, V. M. (1983), Plasma distribution and flow, in *Physics of the Jovian Magnetosphere*, edited by A. J. Dessler, pp. 395–453, Cambridge Univ. Press, New York.

Waite, J. H., Jr., et al. (2001), An auroral flare at Jupiter, *Nature*, *410*, 787–789.

Woch, J. N., et al. (1999), Plasma sheet dynamics in the Jovian magnetotail: Signatures for substorm-like processes?, *Geophys. Res. Lett.*, *26*(14), 2137–2140.

Woch, J., N. Krupp, and A. Lagg (2002), Particle bursts in the Jovian magnetosphere: Evidence for a near-Jupiter neutral line, *Geophys. Res. Lett.*, *29*(7), 1138, doi:10.1029/2001GL014080.

J. T. Clarke, Center for Space Physics, Boston University, 725 Commonwealth Avenue, Boston, MA 02215, USA. (jclarke@bu.edu)

J.-C. Gérard and D. Grodent, LPAP, Université de Liège, Allée du 6 Aout, 17 (B5c), B4000- Liège, Belgium. (d.grodent@ulg.ac.be)

G. R. Gladstone, Southwest Research Institute, 6220 Culebra Road, San Antonio, TX 78238-5166, USA. (randy@whistler.space.swri.edu)

J. H. Waite Jr., Space Physics Research Laboratory, University of Michigan, Ann Arbor, MI 48109-2143, USA. (hunterw@umich.edu)

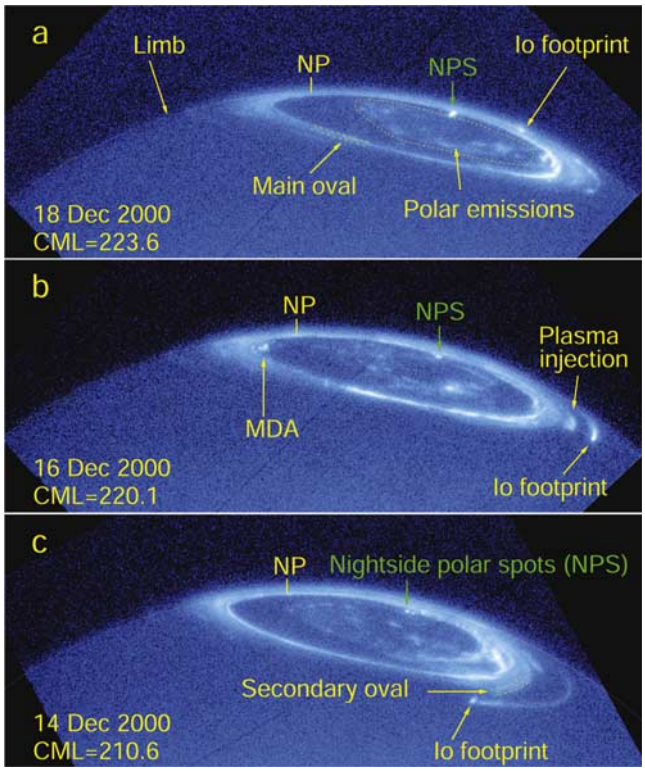

Figure 1. HST-STIS images of the northern polar region of Jupiter showing the new auroral feature, which we refer to as nightside polar spots (NPS) (indicated by an arrow). The three far-UV images were taken on (a) 18 December 2000, (b) 16 December 2000, and (c) 14 December 2000. They were accumulated for ~100 s with the FUV-MAMA Clear aperture. The CML is about 220° for each image, so that the auroral morphologies are very similar, apart from the Io footprint, which has a period of 42 hours. The main oval, the secondary oval, and the polar emissions are located with dashed lines and/or arrows. The plasma injection signature and the multiple dawn arcs (MDA) are visible in Figure 1b only. The north pole (NP) is marked with a vertical tick, and the planetary limb is highlighted with a thin dotted line.

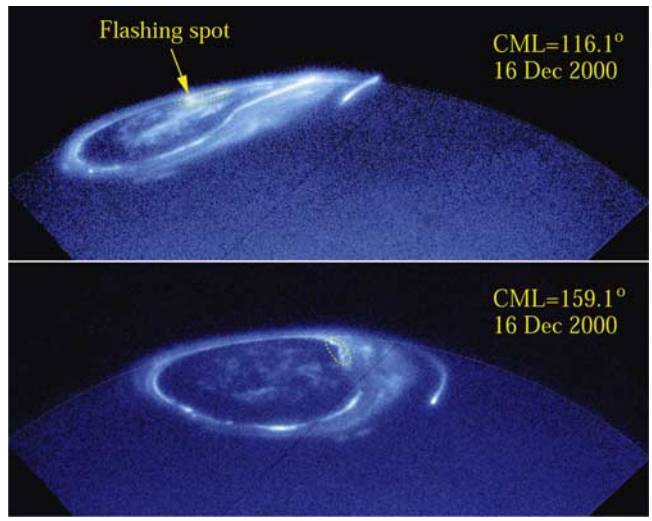

Figure 6. HST-STIS images of the northern auroral region of Jupiter obtained on 16 December 2000 at two different CMLs. The emission spots enclosed in the dotted contours ("flashing spot" for the top panel) are magnetically mapped to the premidnight tail region, beyond 100 R_J, and may therefore represent possible NPS signatures, similar to those observed at CML close to 220° in Figure 1.